NJC

Accepted Manuscript

This is an *Accepted Manuscript*, which has been through the Royal Society of Chemistry peer review process and has been accepted for publication.

Accepted Manuscripts are published online shortly after acceptance, before technical editing, formatting and proof reading. Using this free service, authors can make their results available to the community, in citable form, before we publish the edited article. We will replace this *Accepted Manuscript* with the edited and formatted *Advance Article* as soon as it is available.

You can find more information about *Accepted Manuscripts* in the Information for Authors.

Please note that technical editing may introduce minor changes to the text and/or graphics, which may alter content. The journal's standard Terms & Conditions and the Ethical guidelines still apply. In no event shall the Royal Society of Chemistry be held responsible for any errors or omissions in this *Accepted Manuscript* or any consequences arising from the use of any information it contains.

ROYAL SOCIETY OF CHEMISTRY

www.rsc.org/njc

Study of the electrochemical behavior at low temperature of $Li_3V_2(PO_4)_3$ cathode material for Li-ion batteries

Ling-Hua Tai[1], Qin Zhao[1], Li-Qun Sun[1], Li-Na Cong[1], Xing-Long Wu[1], Jing-Ping Zhang[1], Rong-Shun Wang[1], Hai-Ming Xie[1]*, Xiao-Hong Chen[2]*

[1]*National & Local United Engineering Laboratory for Power Batteries, Department of Chemistry, Northeast Normal University, Changchun, Jilin 130024, PR China*

[2]*College of Chemistry and Chemical Engineering, Inner Mongolia University for the Nationalities, Tongliao 028043, PR China*

Abstract

In this paper, glucose and carbon nanotubes (CNTs) modified $Li_3V_2(PO_4)_3$ have been synthesisd via a carbon thermal reduction method. The structure of $Li_3V_2(PO_4)_3$ has been confirmed by X-ray diffraction, Raman spectra, X-ray photoelectron spectroscopy, scanning and transmission electron microscopy. The CNT modified $Li_3V_2(PO_4)_3$ materials combined with the synthesized electrolyte, overcomes the limitations of Li-ion battery at low temperature. The synthesized electrolyte is made up of 1.2 M $LiPF_6$ dissolved in EC:DMC:EMC (1:1:1 in volume) with vinylene carbonate (VC) and propylene sulfite (PS) as the additive agents. The electrochemical behaviors of the cells have been evaluated by electrochemical test over the temperature range from 25 to −20 °C. The specific capacity is 116.2, 108.2, 103.7, 96.3, 86.1 mAh g^{-1} at 0.5 C, 1 C, 2C, 5 C, 10C between 3.0 and 4.3 V at −20 °C. After 300 cycles the capacity retention still reached 97% even at −20 °C. The excellent rate capability and low

temperature performance are attributed to the synergistic effect between the CNTs and the synthesized low temperature electrolyte.

Keywords: Lithium vanadium phosphate; Carbon-nanotube; Low temperature performance; Lithium ion battery

1. Introduction

Rechargeable lithium ion batteries (LIBs) have been developed as promising energy storage devices for hybrid electric vehicles (HEV) and electric vehicles (EV) owing to their high capacity, high safety, fast charge-discharge rate and long lifespan.[1-3] But the poor electrochemical performance of Li-ion batteries at low temperature is one of the major technical barriers to their application. At −20 °C, the capacity retention of $LiFePO_4$, $LiNi_{1/3}Co_{1/3}Mn_{1/3}O_2$ has only less than 50%.[4, 5]

Monoclinic $Li_3V_2(PO_4)_3$ (LVP) has been proposed as one of the most promising cathode materials for lithium-ion batteries due to its good thermal stability, high security, wide working temperature range, large capacity.[6-9] LVP containing three mobile Li ions can extract and insert two lithium ions reversibly between 3.0 and 4.3 V with a capacity of 133 mAh g^{-1}. When charged to 4.8 V, all the three Li ions can be removed getting a total capacity of 197 mAh g^{-1}. Moreover, Li^+ diffusion coefficient of LVP (i.e., 10^{-9}–10^{-10} cm^2 S^{-1}),[10] is six order of magnitude higher than that of $LiFePO_4$ (i.e., 10^{-14}–10^{-16} cm^2 S^{-1}).[11] No matter at room temperature or low temperature, LVP always can maintain high lithium ion conductivity. Therefore LVP is a highly suitable candidate for the cathode of LIBs at low temperature.[12-17] However, the electronic conductivity

of LVP is the main limiting factor of the cathode material. Carbon coating, [9, 18-21] cation doping in vanadium site[22-26] and decreasing the particle size[27-29] have been proved to be effective to enhance the intrinsic electronic conductivity. The above methods can enhance the capacity retention and rate performance.

Generally, carbon coating is one of the most effective methods to improve the electronic conductivity. The uniformity of carbon coating is crucial to achieve high electronic conductivity and lithium ion mobility. As a kind of special carbon, CNTs have shown great potential in Li-ion battery materials due to their peculiar structure and unique properties such as chemical stability, tensile strength and flexibility.[20, 30-32] Jegal's group has reported the positive effect of CNTs on the electrochemical performance of $LiFePO_4$,[33] which show a superior rate capacity and excellent cycle performance owing to the cross-linked structure and the high electronic conductivity of CNTs. Here, the low temperature performance of LVP has been effectively improved by CNTs modified.

Electrolyte is also one of the major factors that affect the performance of battery, especially at low temperature. EC:DMC electrolyte has a wide electrochemical stability window and good cycle life at room temperature, but it cannot operate below −20 °C normally. The reason for that is the solidification of the EC component at low temperature in the binary solvent systems, which worsens the ions separation in solution and the ions' mobility.[34] To improve the performance of the electrolyte at low temperature, multiple strategies are adopted. Firstly, more than two solutions used in electrolyte can permit an optimization of the electrolyte properties, like liquid range,

viscosity and dielectric constant especially at low temperature. Secondly, increasing the concentration of lithium salt ensure more Li^+ ions transference number in the electrolyte. Finally, adding electrolyte additives, which is helpful to reduce electrode polarization and improve the low temperature performance of the electrolyte. Up to now, much research has been published on the electrolyte additives. One is low-temperature co-solvent like methyl ester, methyl acetate, ethyl acetate, mono-fluoroethylene carbonate and so on, which can decrease the melting point of the electrolyte. The other is film-forming additives, for example, sulfite (ethylene sulfite and propylene sulfite) and carbonate (vinylene carbonate), [35-37] which can form lower impedance and a stable surface film between the electrolyte and the cathode improving the safety and cycling stability. Incorporating these additives into electrolyte is also beneficial to widen the operating temperature of these systems.

In this work, CNTs modified cathode material combining the optimized electrolyte are introduce to improve the electrochemical performance of Li-ion battery at low temperature. The structure, surface character and electrochemical performance of CNT modified $Li_3V_2(PO_4)_3$ materials at low temperature are systematically investigated in the traditional and the synthesized electrolytes, respectively .

2. Experimental

2.1 Material preparation

The double carbon decorated LVP composite (LVP@C/CNT) was synthesized by ball-milling and carbon-thermal reduction method. A mixture of $LiOH{\cdot}H_2O$, NH_4VO_3,

$NH_4H_2PO_4$ in stoichiometric molar ratio (3:2:3) were mixed together with 10 wt% glucose and CNTs (CNTs were ultrasonic treatment with ethanol, Shenzhen Nanotech Port Co., Ltd) and ground by ball milling for 8 h. The weight ratio of glucose and CNT is 1:1. The rotation speed was 500 rpm. After the ethanol was completely evaporated at 70 °C, the precursor was collected and pre-sintered at 350 °C for 4 h and subsequently sintered at 750 °C for 8 h under N_2 gas atmosphere in a tube furnace. The schematic diagram of the synthesis process was shown in Scheme 1. For comparison, the sample of LVP only with glucose as carbon source (LVP@C) was prepared in the same way.

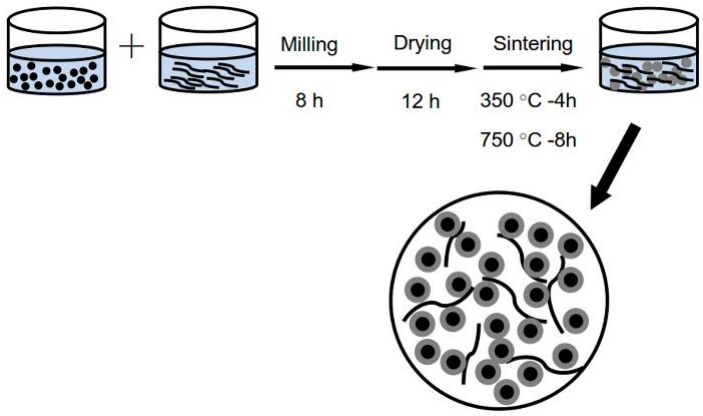

Scheme 1 Schematic diagram of the synthesis process of the LVP@C/CNT

2.2 Material characterization

The crystalline phase was identified by X-ray diffraction (XRD; Rigaku-Dmax2500) using Cu *Kα* radiation in the 2*θ* range of 10−70° at room temperature. Raman spectra were taken by a RM1000/SNOM100 with a 50× objective lens and 514.5 nm laser excitation. The power morphologies were examined using scanning electron microscopy (SEM; XL30) and transmission electron microscopy (TEM; JEOL

2100F). The thermogravimetric analysis (TGA) was conducted in air at a heating rate of 10 °C/min using a thermal analyzer (Shimadzu TGA60H). The four-point probe resistivity measurement system is used to measure the electronic conductivities of the two composites X-ray photoelectron spectroscopy (XPS) was acquired by using an ESCALab220i-XL spectrometer. Nitrogen adsorption measurements were performed at 77 K using a Micromeritics ASAP 2020 M adsorption analyzer.

2.3 Electrochemical tests

Electrochemical measurements were carried out using CR2025 coin cells. The working electrodes were made by blending 80 wt% of the active material with 10 wt% of acetylene black and 10 wt% of polyvinylidene difluoride (PVDF) as a binder in N-methyl-2-pyrrolidone. The obtained slurry was pasted onto aluminum foil and dried at 120 °C for 12 hours in vacuum. Lithium metal was used as the anode. The electrolyte was 1.2 M $LiPF_6$ in ethylene carbonate (EC)/dimethyl carbonate (DMC)/ethyl methyl carbonate (EMC) with a volume ratio of 1:1:1. And vinylene carbonate (VC) and propylene sulfite (PS) were used as electrolyte additives. For comparison, the electrolyte with 1.0 M $LiPF_6$ in ethylene carbonate (EC)/dimethyl carbonate (DMC) was prepared in the same way. Cells were assembled in an argon-filled glove box. The coin cells were cycled galvanostatically in the voltage ranges 3.0−4.3 V. And also tested at various temperatures 25, 0, −10, −20 °C under a constant current density of 0.5 C. Cyclic voltammetry (CV) was conducted using an electrochemical workstation (CHI606B) at different scan rates of 0.1, 0.2, 0.5, 0.8 mV s^{-1}. Electrochemical

impedance spectroscopy (EIS) was also recorded on a Par 2273 Potentiostats-Electrochemical Workstation with sinusoidal signal of 5 mV over a frequency range from 100 kHz to 10 mHz. The Tafel polarization curves at −20 °C were measured under potentiodynamic conditions using scan rate of 0.166 mV s^{-1}. The cathodes were adopted as the work electrode; the counter electrode and reference electrode were Li foil.

3. Results and discussion

3.1 Physical and chemical characterization

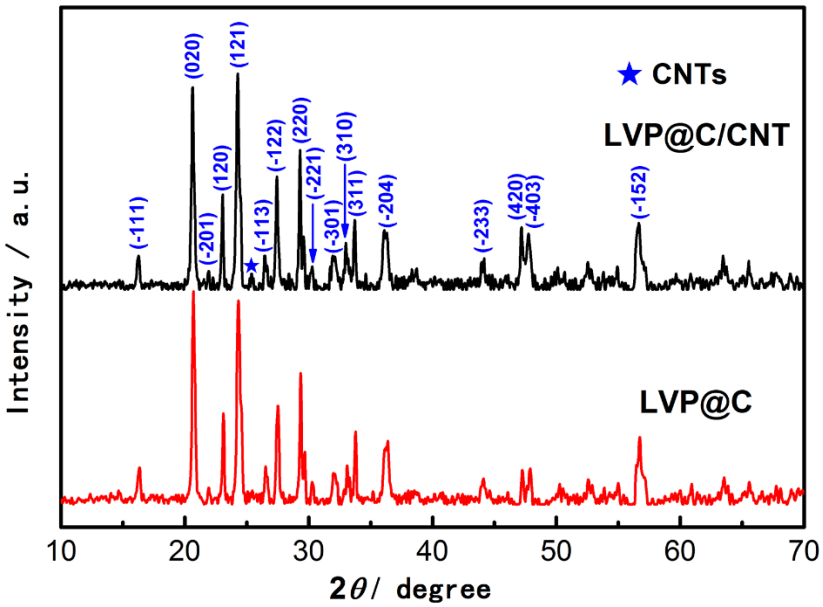

Fig. 1 XRD images of LVP@C and LVP@C/CNT

The XRD patterns of LVP@C and LVP@C/CNT are shown in Fig. 1. All the diffraction peaks of them are well indexed to be the monoclinic LVP with a space group of $P2_1/n$. The peaks in XRD patterns are also in good agreement with the other reported

literatures[38-41] except for a small peak appeared in LVP@C/CNT compound at 25.5 °, which is attributed to the (002) plane of multiwall CNT.[42] No evidence of carbon is detected in LVP@C sample, suggesting that the residual carbon is amorphous or the concentration of the residual carbon is too low to be detected.

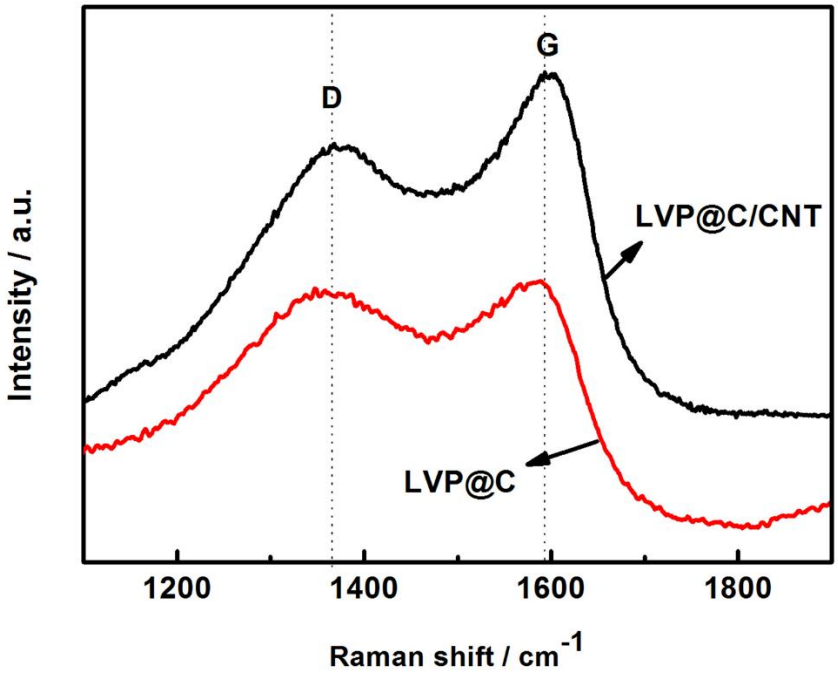

Fig. 2 Raman spectra of LVP@C and LVP@C/CNT

Fig. 2 shows the Raman spectra of LVP@C and LVP@C/CNT. The bands at 1363 cm^{-1} and 1595 cm^{-1} are attributed to the D-band (disorder-induced phonon mode) and G-band (graphite band) of carbon, respectively. The D and G fractions of the composites were estimated by fitting the Raman spectra. Each component is a convolution of a Gaussian distribution, and the contribution of the background was subtracted by using the Shirley method. The integral intensity ratios of the D band to the G band for LVP@C and LVP@C/CNT were estimated to be about 0.96 and 0.86,

respectively, indicating the relatively high degree of graphitization of LVP@C/CNT due to the 3D network structure of CNT. The lower D/G ratio of LVP@C/CNT means the better electrical conductivity.

The chemical state and type of the surface carbon of the samples are also analyzed with X-ray photoelectron spectroscopy (XPS). Each component is a convolution of a Gaussian and a Lorentzian method, and the contribution of the background is approximated by the Shirley method. As shown in Fig. 3 (a), the peaks at 284.56, 285.85 and 288.61 eV are assigned to the sp^3 carbon (C−C), C−O/C=O bonds and −O−C=O, respectively. The existence of the carboxyl group (−O−C=O) attributes to incomplete decomposition of glucose during the preparation process. In the LVP@C/CNT (Fig 3. (b)), the binding energy peaks corresponding to the sp^3 carbon (C−C) and C−O/C=O bonds are the same as those clearly visible in the spectra of the LVP@C. It is noteworthy that the peak appeared at 284.48 eV is corresponding to the sp^2 carbon (C=C) coming from the CNTs, which indicates the relatively high degree of graphitization of LVP@C/CNT. This is consistent with the results of the XRD and Raman tests.

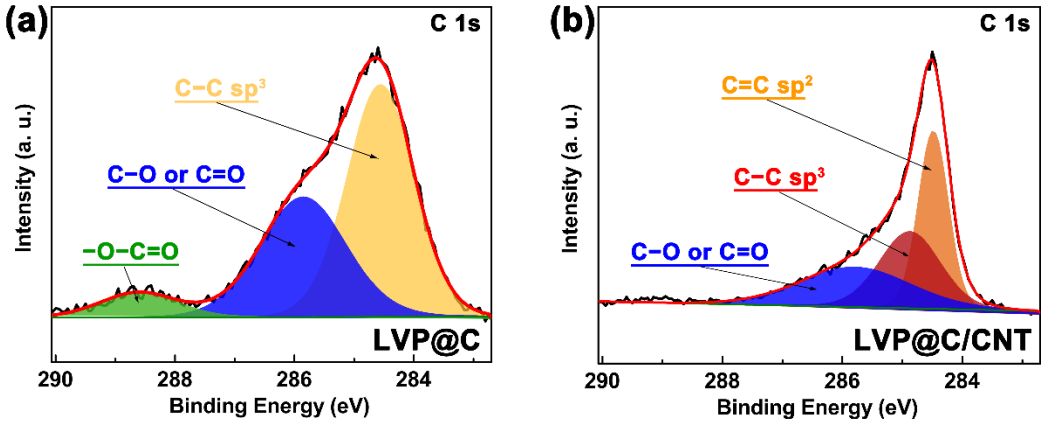

Fig. 3 The X-ray photoelectron spectroscopy (XPS) of the C 1s of the LVP@C (a), LVP@C/CNT (b).

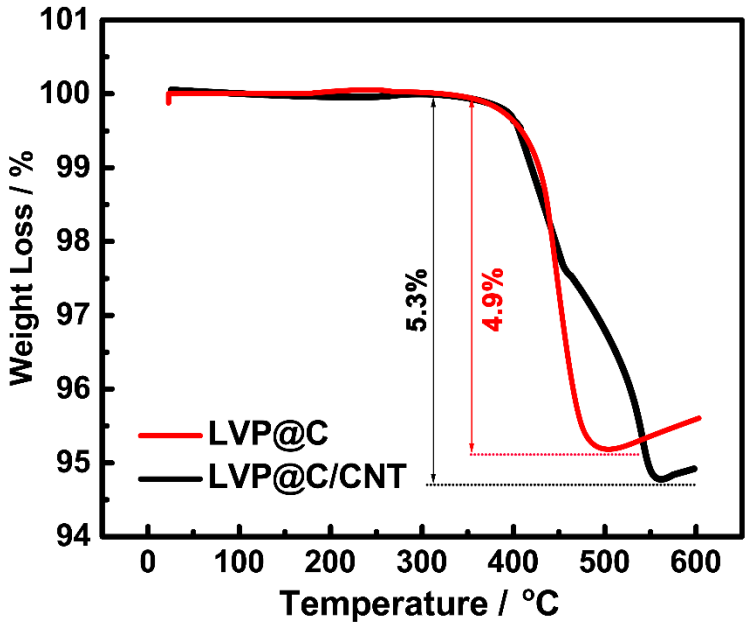

Fig. 4 TGA curves of LVP@C, and LVP@C/CNT composites.

To speculate the carbon contents of the samples LVP@C and LVP@C/CNT accurately, the thermogravimetric analysis were carried on in air at a heating rate of 10 °C min^{-1} from 25 °C to 600 °C using a thermal analyzer (TGA60H), separately (Fig. 4). The composites initially undergo a weight loss in the temperature range of 400−550°C, which is attributed to the burnout of the residual carbon. The following weight gain step is due to the decomposition of $Li_3V_2(PO_4)_3$, corresponding to the oxidation of V^{3+} in air. According to the weight loss step on the TGA curves, the carbon content of LVP@C, and LVP@C/CNT are 4.9%, 5.3%, respectively.

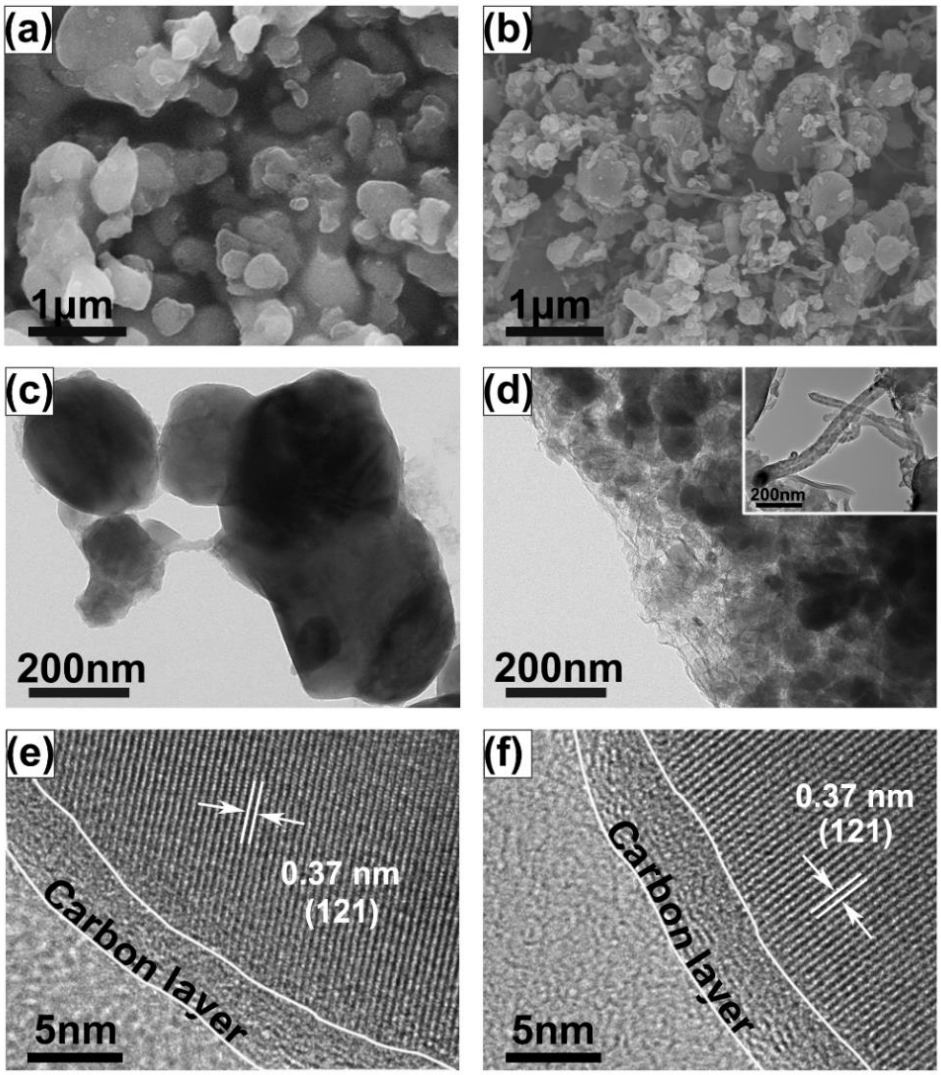

Fig. 5 SEM images of LVP@C (a) and LVP@C/CNT (b). TEM images of LVP@C (c) and LVP@C/CNT (d), HRTEM images of LVP@C (e) and LVP@C/CNT (f)

The morphologies and microstructures of LVP@C and LVP@C/CNT composites are shown in Fig. 5. It is observed that a certain degree of agglomeration of the primary particle is observed in LVP@C sample (Fig. 5a, 5c), while LVP@C/CNT has more uniform particle distribution and smaller particle size (~150 nm) (Fig. 5b, 5d) than LVP@C (~300 nm). The CNTs distributed between the LVP nanoparticles can effectively prevent the growth and gathering of the particles and form more structure

pores and aggregation pores (Fig. 5d), which is benefit to improve the Li ion mobility and ensure the high reversibility of Li ion intercalation and de-intercalation at low temperature. To further investigate the microstructure of the samples, the typical HRTEM images of LVP@C and LVP@C/CNT composites are shown in Fig. 5e and 5f. The observed width (0.37 nm) of the neighboring lattice fringes in the HRTEM images corresponds to the (121) plane of LVP, demonstrating the well-textured and crystalline nature of LVP particles in the LVP@C and LVP@C/CNT. From the images, a uniform amorphous carbon coating with a thickness of about 3−4 nm can be observed on the surfaces of both samples.

Nitrogen adsorption–desorption isotherms were also carried out to confirm the microstructure of the samples, as shown in Fig. 6. The nitrogen adsorption and desorption curves showed the present of hysteresis loops which is the characteristic feature of Type IV isotherm. The BET surface area of LVP@C/CNT (21.96 m^2/g) is larger than that of LVP@C(11.53 m^2/g), which further demonstrates that an optimum 3D conducting network structure was formed in the LVP@C/CNT sample by one-dimensional CNTs winding. It is also consistent with the results of the SEM and TEM results.

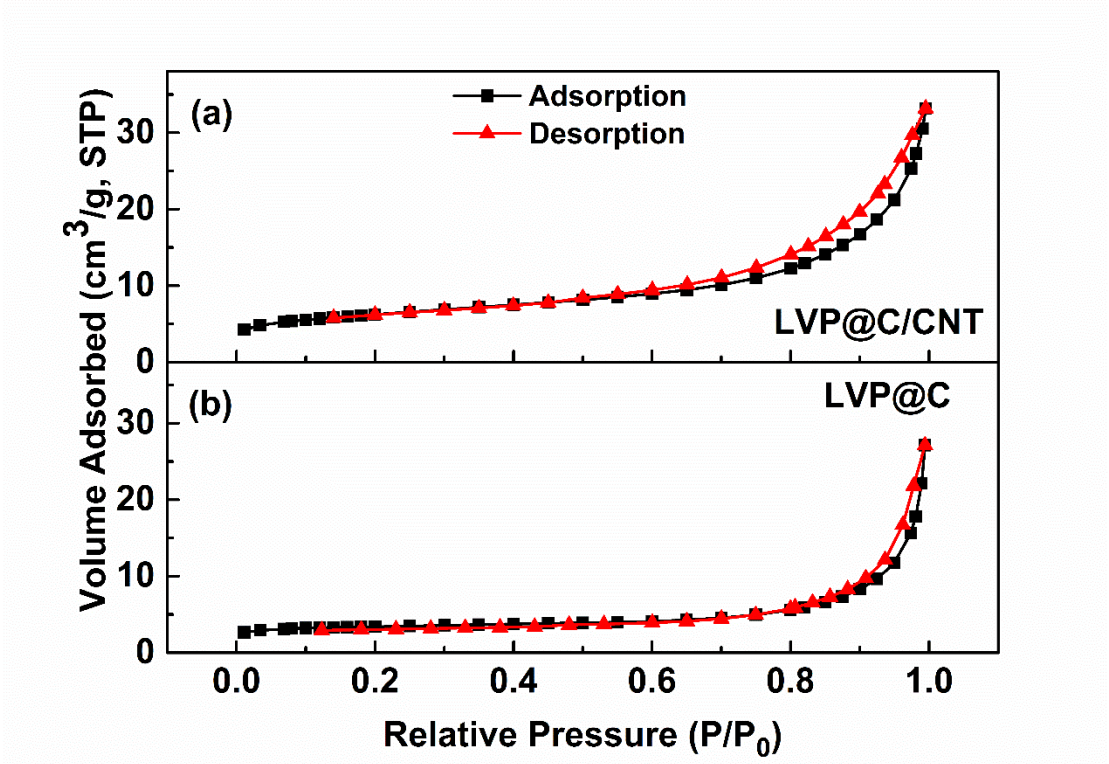

Fig. 6 Nitrogen adsorption−desorption isotherm of LVP@C/CNT (a), LVP@C (b).

Meanwhile, the CNTs with high conductivity and excellent mechanical properties can also act as the electronic conducting path in LVP@C/CNT. The electronic conductivities of the composites were measured on a four-point probes resistivity measurement system. LVP@C/CNT presents the higher electronic conductivity (1.2×10^{-2} S cm^{-1}) than that of LVP@C (4.9×10^{-4} S cm^{-1}).

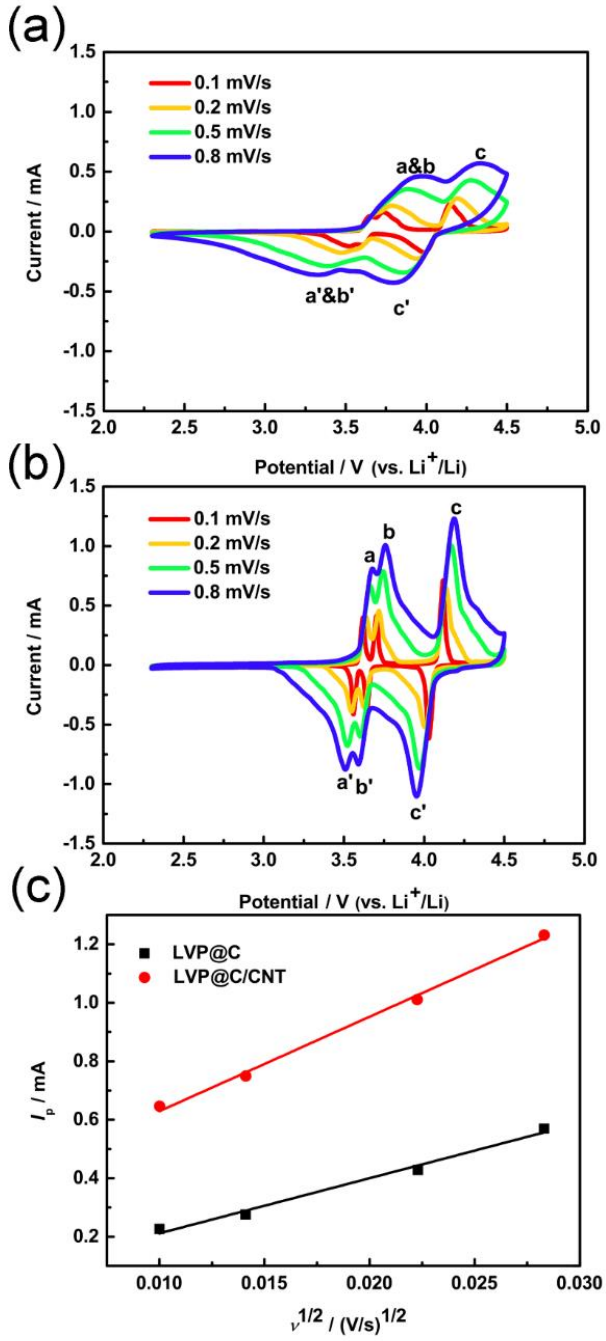

Fig. 7 Cyclic voltammetry at different sweep rates for LVP@C (a) and LVP@C/CNT (b). Relationship of the c peak current (I_p) and the square rate ($v^{1/2}$) for LVP@C and LVP@C/CNT material (c)

3.2 Electrochemical characterization

Fig.7 illustrate cyclic voltammograms (CV) curves of the LVP@C and LVP@C/CNT samples in $LiPF_6$ EC:DMC (1:1 in volume) at room temperature using a scanning rate of 0.1, 0.2, 0.5, 0.8 mV s^{-1}. Both of them have three pairs of anodic and cathodic peaks in the range of 2.3−4.5 V, which represent the Li^+ de-intercalation and re-intercalation process. Three couples of anodic and the corresponding cathodic peaks of LVP@C appear around 3.64, 3.73, 4.15 and 3.52, 3.60, 3.98 V respectively (Fig. 7a). However, in the case of LVP@C/CNT, the oxidation peaks appear at 3.61, 3.70, 4.12 V shifting to the lower potential, while the reduction peaks appear at 3.56, 3.64, 4.02 V shifting to the higher potential, respectively (Fig. 7b). It indicates that CNTs enhanced the electrode reaction reversibility and lower the polarization of LVP@C/CNT. The LVP@C/CNT cathode still undergoes three complete phase transitions at high scanning rates while a (a′) and b (b′) peaks of LVP@C are amalgamated into one peak. In addition, the current of LVP@C/CNT is much higher than that of LVP@C, indicating its high reversibility during electrochemical reaction. For the semi-infinite and finite diffusion, the peak current is proportional to the squareroot of the scanning rate and can be expressed by the classical Randles Sevchik equation:[43]

$$I_p = 2.69 \times 10^5 n^{3/2} A C D^{1/2} v^{1/2} \quad (1)$$

Where I_p is the peak current (A), n is the number of electrons per species reaction, A is the active surface area of the electrode (cm^{-3}), C is the concentration of lithium ions in the cathode (mol cm^{-3}), D is the apparent ion diffusion coefficient (cm^2 s^{-1}), and v is the scanning rate (V s^{-1}). As shown in Fig. 7c, I_p is indeed proportional to $v^{1/2}$ confirming the diffusion-controlled behavior. Based on the slope of I_p vs. $v^{1/2}$, and Eq.

(1), the apparent diffusion coefficients D_c (peak c) are calculated. The values are 6.4×10^{-10} and 3.0×10^{-9} cm^2 s^{-1} for LVP@C and LVP@C/CNT (Fig. 7c). The result clearly indicates that the lithium ion mobility of LVP@C/CNT can be effectively improved by CNTs. It is consistent with the results of previous analysis.

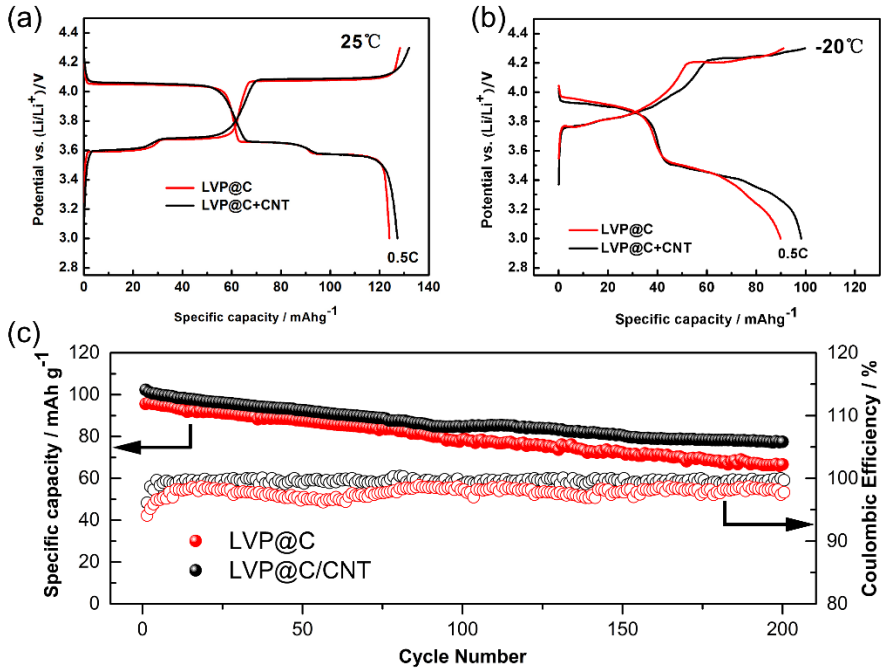

Fig. 8 Charge-discharge profiles of LVP@C and LVP@C+CNT between 3.0−4.3V at 25 °C (a) and −20 °C (b). The cycle performance and coulombic efficiency of LVP@C and LVP@C+CNT at the rate of 0.5 C at −20 °C (c)

Fig. 8a and b display the initial charge/discharge curves of LVP@C and LVP@C/CNT at 25 °C and −20 °C. As seen from the curves, there are three charge flat plateaus (around 3.65, 3.73 and 4.15 V) and three discharge flat plateaus (around 3.51, 3.60, 4.02 V), agreeing with the CV results. The specific capacity of LVP@C/CNT is 127.3 mAh g^{-1}, which is a little larger than that of LVP@C (124.0 mAh g^{-1}) at 0.5 C

under 25 °C. At room temperature, all the plateaus can be observed clearly in both samples. When the temperature decreases from 25 to −20 °C, the plateaus became vague. The capacities are reached 101.6 mAh g^{-1} for LVP@C/CNT and 90.8 mAh g^{-1} for LVP@C. Despite the capacities of the two samples are both decreased, the capacity retention of LVP@C/CNT can still retain 76.5% after 200 cycles at −20 °C. Compared with LVP@C/CNT, the capacity of LVP@C drops obviously and the capacity retention is only 70.5% (Fig. 8c).

Therefore, CNTs coating layer reinforce the connection between the LVP@C nanoparticles, which are benefit to form an optimal three-dimensional conducting network and obtain a better electron transportation path, and also shorten the ion diffusion length and improve the Li ion mobility, ensuring the high reversibility of Li ion intercalation and de-intercalation at low temperature.

Although the specific capacity of LVP at low temperature can be improved by CNTs modified, the electrochemical polarization of LVP@C/CNT is quite obvious at −20 °C (Fig. 8b). Thus, the functional electrolyte plays an important role to the low temperature performances of lithium ion battery. Two kinds of electrolytes are adopted to assemble the coin cells with the LVP@C/CNT composite as the cathode material. One is the traditional electrolyte of 1.0 M $LiPF_6$ EC:DMC (1:1 in volume) abbreviated LVP@C/CNT (1#), the other is the optimized electrolyte of 1.2 M $LiPF_6$ EC:DMC:EMC (1:1:1 in volume) with VC and PS as additives abbreviated LVP@C/CNT (2#).

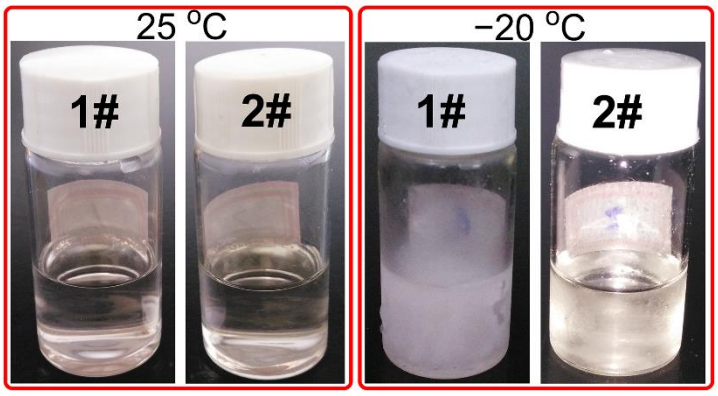

Fig. 9 Photos of the electrolytes 1# and 2# at different temperature

To compare the physical state of the two electrolytes at different temperatures, they were put into the ice box for 5 hours at −20 °C. The photos of the two electrolytes at different temperatures can be seen in Fig. 9. There is no obviously difference to both of the electrolytes at 25 °C, however, LVP@C/CNT (1#) is frozen after 5 h at −20 °C, while LVP@C/CNT (2#) is still keeping good mobility. Thus, increasing the components of electrolyte by adding electrolyte additives can widen liquid range and improve the mobility of the electrolyte.

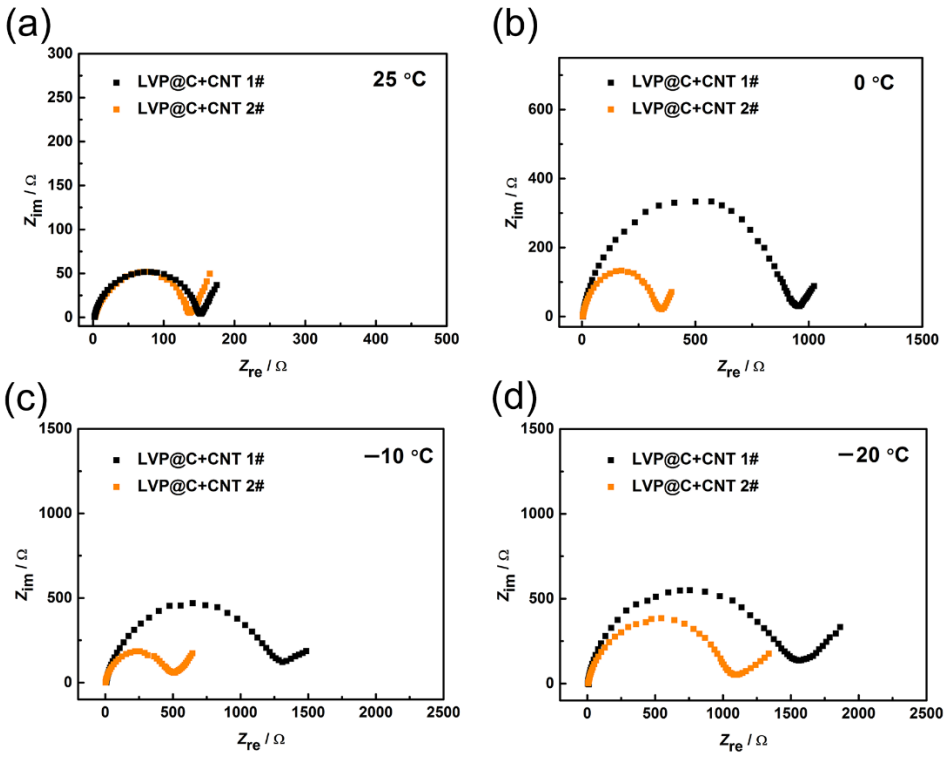

Fig. 10 Nyquist plots of LVP@C/CNT (1#) and LVP@C/CNT (2#) measured after 1 cycle at 25 °C (a), 0 °C (b), −10 °C (c), −20 °C (d)

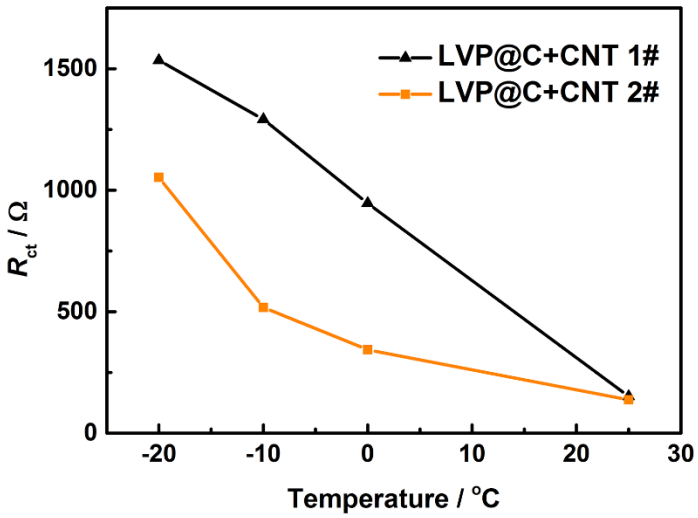

Fig. 11 The series resistance derived from EIS over a wide range of temperature containing various electrolytes

To understand the kinetics of the electrode in two different electrolytes, the Nyquist plots of LVP@C/CNT at different operation temperature are shown in Fig. 10. It is apparently seen that the impedance spectrum is composed of overlapped semicircle at high-middle frequency regions, and a straight slopping line at low frequency. The semicircle in the high-middle frequency region represents charge-transfer resistance (R_{ct}), the straight line in the low-frequency region is attributed to the diffusion of the lithium ions into bulk of electrode material. As shown in Fig. 10, the charge-transfer resistances of the cells increase with decreasing temperature. It directly demonstrates that the LVP@C/CNT (2#) has much lower charge resistance (R_{ct} = 1032.2 Ω) than the LVP@C/CNT (1#) (R_{ct} = 1582.4 Ω). The series resistance is derived from EIS over a wide range of temperature containing two different electrolytes (Fig. 11). VC and PS additives have improved the mass transfer characteristics of the electrolyte at low temperature and further increase the electrons and Li ions migration rate.

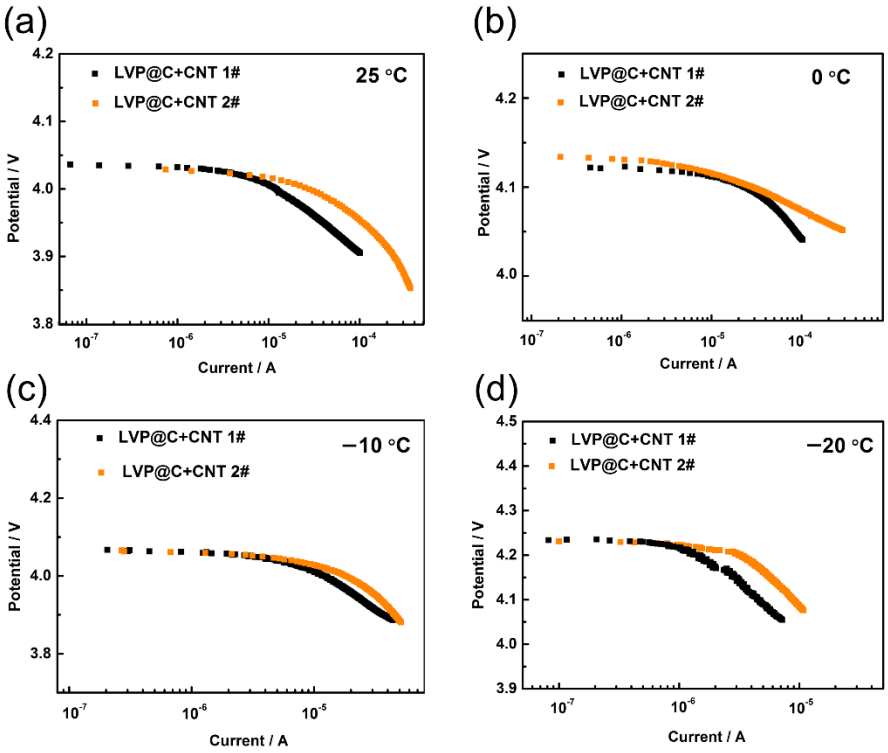

Fig. 12 Tafel polarization measurements at 25 °C (a), 0 °C (b), −10 °C (c), −20 °C (d) of LVP@C/CNT (1#) and LVP@C/CNT (2#)

The lithiation/delithiation kinetics were determined for the cathodes by conducting Tafel polarization measurements of the LVP@C/CNT in contact with the two electrolytes. In all of the Tafel plots, the regimes of overpotential increase linearly with log(*I*) represents charge-transfer controlled regimes, and the exchange current densities can be calculated from the intercept of log(*I*) on the equilibrium voltage.[44] The trends with regard to the observed lithium kinetics and how they depend upon electrolyte type tend to track well with temperature. As illustrated in Fig. 12, the Tafel polarization measurements have been performed on the LVP@C/CNT cathodes at different temperature. According to the value of exchange current densities, improved lithium de-intercalation kinetics (i.e., higher limiting current) were observed for the cathodes

LVP@C/CNT in contact with the VC and PS electrolyte additives compared to the system that does not contain the additives. The exchange current density of the cells of LVP@C/CNT (2#) is 2.98×10^{-3} mA cm^{-2}, which is higher than that of LVP@C/CNT (1#) (0.96×10^{-3} mA cm^{-2}) at −20 °C, implying an improved electrochemical reaction rate or a reduction in charge−transfer resistance due to the modified electrolyte. This is maybe another reason for the improved low temperature performance of LVP@C/CNT (2#).

Table 1 The comparison of capacity of the LVP@C/CNT in different electrolyte at 25 °C

	0.5C	**1C**	**2C**	**5C**	**10C**
LVP@C/CNT (1#) (mAh g^{-1})	127.2	119.7	120.5	115.4	111.5
LVP@C/CNT (2#) (mAh g^{-1})	128.3	123.3	120.6	119.6	112.2

Table 2 The comparison of capacity of the LVP@C/CNT in different electrolyte at −20 °C

	0.5C	**1C**	**2C**	**5C**	**10C**
LVP@C/CNT (1#) (mAh g^{-1})	103.1	90.3	79.0	67.5	56.8
LVP@C/CNT (2#) (mAh g^{-1})	116.2	108.2	103.7	96.3	86.1

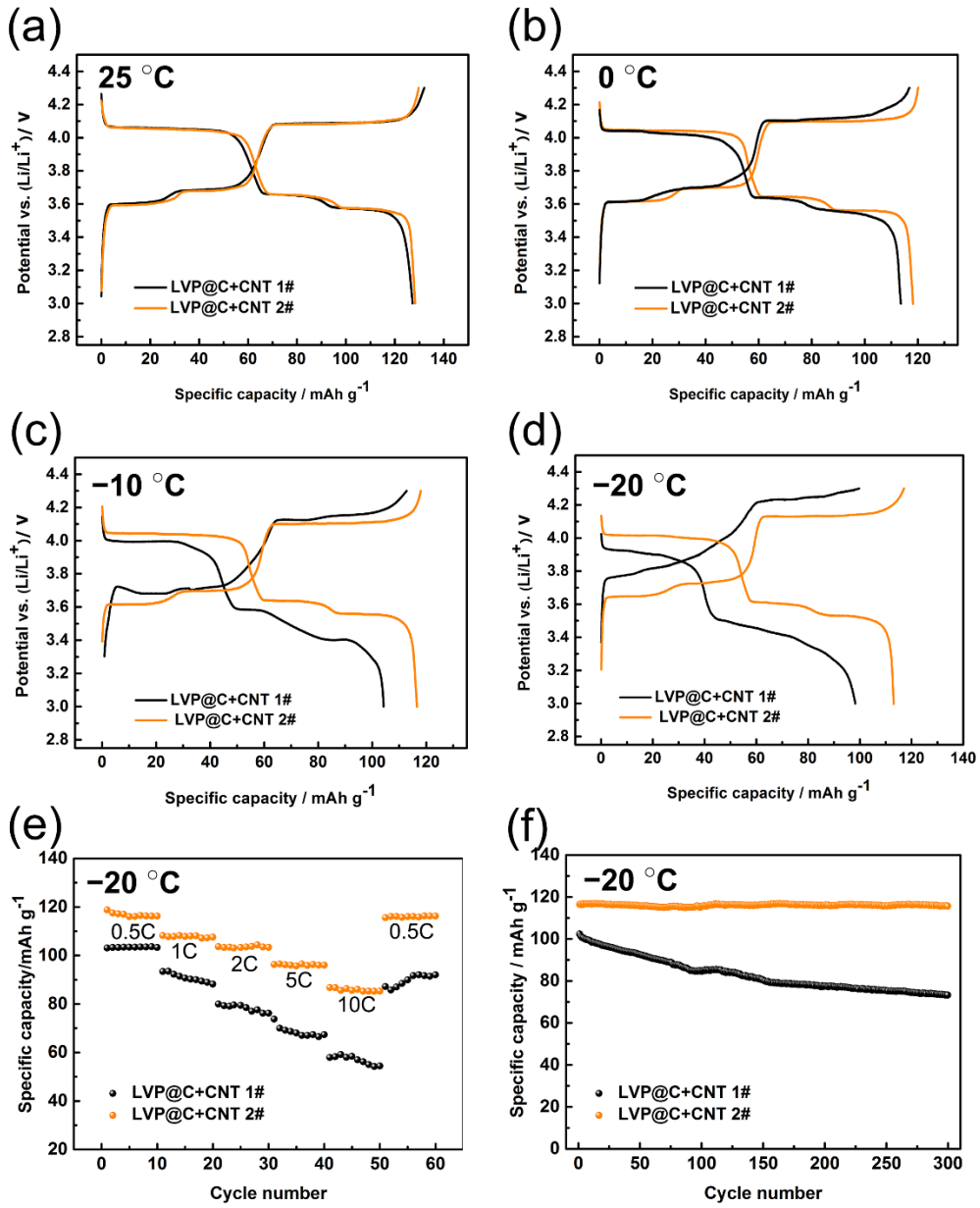

Fig. 13 The charge/discharge curves of LVP@C/CNT (1#) and LVP@C/CNT (2#) at the rate of 0.5 C at 25 °C (a), 0 °C (b), −10 °C (c) and −20 °C (d). The rate performance (e) and cycle performance profiles (f) of the materials at 0.5 C rate at −20 °C.

The electrochemical performance of the initial charge and discharge profiles at different temperatures are shown in Fig. 13 a~d. The LVP@C/CNT (2#) delivers an average discharge capacity of 128.3 mAh g^{-1} at 0.5 C rate at room temperature, which

is higher than that of LVP@C/CNT (1#) (127.2 mAh g^{-1}) (Fig. 13a). The capacities of the two samples at 25 °C at different rates are listed in Table 1. The difference of the capacities is not obvious at room temperature. When the operating temperature drops to the critical temperature range, the electrochemical performance shows significant differences. The discharge capacities of LVP@C/CNT (2#) reached 120.1, 118.6, 113.5 mAh g^{-1}, which are much higher than that of LVP@C/CNT (1#) at 0, −10, −20 °C, respectively (Fig. 13b~d). It also can be seen that the capacity of the LVP@C/CNT (1#) decreases gradually with the temperature decreasing and the plateaus also become unstable and only one plateau is left in particular at −20 °C in the range of 3.4~3.6V. However, the curves of LVP@C/CNT (2#) maintain stable at −20 °C, as shown in Fig. 13d, and two plateaus appear obviously at 3.6V and 3.4V, separately, implying the polarization decreased by VC and PS additives at low temperature. Fig. 13e shows the rate capabilities of LVP@C/CNT (1#) and LVP@C/CNT (2#) at −20 °C. LVP@C/CNT (2#) delivers the discharge capacities of 116.2, 108.2, 103.7, 96.3, 86.1 mAh g^{-1} at 0.5 C, 1 C, 2C, 5 C, 10C respectively, which is much higher than that of LVP@C/CNT (1#) (Table 2). The cycle performance of LVP@C/CNT (2#) also displayed much better than that of LVP@C/CNT (1#) at 0.5 C in the range of 3.0~4.3 V at −20 °C (Fig. 13f). The specific capacity of LVP@C/CNT (2#) is up to 113.2 mAh g^{-1} after 300 cycles with the capacity retention of 97%. The excellent performances of the LVP@C/CNT (2#) sample could be due to the 3D conductive network structure of the sample composed by the uniform nanoparticles and CNTs winding technology, combining the optimized electrolyte.

4. Conclusion

In summary, the low temperature performances of the double carbon decorated $Li_3V_2(PO_4)_3$ composite (LVP@C/CNT) were significant improved firstly by the carbon nanotubes (CNTs) modified and further by the optimized electrolyte. The nano-sized LVP@C/CNT particles were embedded inside the special CNTs conductive network preventing the aggregation of the particles and providing excellent electron and lithium ion transmission routes simultaneously. The optimized electrolyte not only reduced the polarization and charge-transfer resistance but also increased the electrochemical reaction rate, and further improved the electrochemical performances of LVP@C/CNT at low temperature.

Acknowledgements

This work was supported by National High Technology Research and Development Program of China (2013AA110103).

References

1. X.-L. Wu, L.-Y. Jiang, F.-F. Cao, Y.-G. Guo and L.-J. Wan, *Adv Mater*, 2009, **21**, 2710-2714.
2. B. Kang and G. Ceder, *Nature*, 2009, **458**, 190-193.
3. L.-L. Zhang, X. Zhang, Y.-M. Sun, W. Luo, X.-L. Hu, X.-J. Wu and Y.-H. Huang, *J Electrochem Soc*, 2011, **158**, A924-A929.
4. X. H. Rui, Y. Jin, X. Y. Feng, L. C. Zhang and C. H. Chen, *J Power Sources*, 2011, **196**, 2109-2114.
5. S. J. Shi, J. P. Tu, Y. Y. Tang, Y. Q. Zhang, X. Y. Liu, X. L. Wang and C. D. Gu, *J Power Sources*, 2013, **225**, 338-346.
6. L. Wang, X. Li, Z. Tang and X. Zhang, *Electrochem Commun*, 2012, **22**, 73-76.
7. C. Wang, W. Shen and H. Liu, *New J Chem*, 2014, **38**, 430-436.

8. W. J. Zhang, Q. J. Liu, L. J. Feng, S. P. Wang, Y. Z. Yang and H. Y. Wei, *New J Chem*, 2014, **38**, 2265-2268.
9. C.L. Fan, S.C. Han, K.H. Zhang, L.F. Li and X. Zhang, *New J Chem*, 2014, **38**, 4336-4343.
10. X. H. Rui, N. Ding, J. Liu, C. Li and C. H. Chen, *Electrochim Acta*, 2010, **55**, 2384-2390.
11. D. Bhuvaneswari and N. Kalaiselvi, *Phys Chem Chem Phys*, 2014, **16**, 1469-1478.
12. Q. Wei, Q. An, D. Chen, L. Mai, S. Chen, Y. Zhao, K. M. Hercule, L. Xu, A. Minhas-Khan and Q. Zhang, *Nano Lett*, 2014, **14**, 1042-1048.
13. H. Liu, P. Gao, J. Fang and G. Yang, *Chem Commun (Camb)*, 2011, **47**, 9110-9112.
14. W. Duan, Z. Hu, K. Zhang, F. Cheng, Z. Tao and J. Chen, *Nanoscale*, 2013, **5**, 6485-6490.
15. L. Mai, S. Li, Y. Dong, Y. Zhao, Y. Luo and H. Xu, *Nanoscale*, 2013, **5**, 4864-4869.
16. H. Huang, S. C. Yin, T. Kerr, N. Taylor and L. F. Nazar, *Adv Mater*, 2002, **14**, 1525-1528.
17. Y. Q. Qiao, J.P. Tu, X.L. Wang and C.D. Gu, *J Power Sources*, 2012, **199**, 287-292.
18. Y. Luo, X. Xu, Y. Zhang, Y. Pi, Y. Zhao, X. Tian, Q. An, Q. Wei and L. Mai, *Advanced Energy Materials*, 2014.
19. J. Wang, X. Zhang, J. Liu, G. Yang, Y. Ge, Z. Yu, R. Wang and X. Pan, *Electrochim Acta*, 2010, **55**, 6879-6884.
20. Y. Q. Qiao, J. P. Tu, Y. J. Mai, L. J. Cheng, X. L. Wang and C. D. Gu, *J Alloy Compd*, 2011, **509**, 7181-7185.
21. Y. Q. Qiao, X. L. Wang, Y. Zhou, J. Y. Xiang, D. Zhang, S. J. Shi and J. P. Tu, *Electrochim Acta*, 2010, **56**, 510-516.
22. C. Deng, S. Zhang, S. Y. Yang, Y. Gao, B. Wu, L. Ma, B. L. Fu, Q. Wu and F. L. Liu, *The Journal of Physical Chemistry C*, 2011, **115**, 15048-15056.
23. W. Wang, J. Zhang, Z. Jia, C. Dai, Y. Hu, J. Zhou and Q. Xiao, *Phys Chem Chem Phys*, 2014, **16**, 13858-13865.
24. Y. Z. Dong, Y. M. Zhao and H. Duan, *J Electroanal Chem*, 2011, **660**, 14-21.
25. L. Liu, X. Lei, H. Tang, R. Zeng, Y. Chen and H. Zhang, *Electrochim Acta*, 2015, **151**, 378-385.
26. C.X. Ma, W.F. Mao, Z.Y. Tang and Q. Xu, *J Solid State Electrochem*, 2015, **19**, 519-524.
27. B. Pei, Z. Jiang, W. Zhang, Z. Yang and A. Manthiram, *J Power Sources*, 2013, **239**, 475-482.
28. X. Zhang, N. Böckenfeld, F. Berkemeier and A. Balducci, *ChemSusChem*, 2014, **7**, 1710-1718.
29. X. Li, W. He, Z. Xiao, F. Peng and J. Chen, *J Solid State Electrochem*, 2013, **17**, 1991-2000.
30. X.-L. Wu, Y.-G. Guo, J. Su, J.-W. Xiong, Y.-L. Zhang and L.-J. Wan, *Advanced*

Energy Materials, 2013, **3**, 1155-1160.
31. D. Morgan, G. Ceder, M. Y. Saïdi, J. Barker, J. Swoyer, H. Huang and G. Adamson, *J Power Sources*, 2003, **119-121**, 755-759.
32. W. F. Mao, Y. B. Fu, H. Zhao, G. Ai, Y. L. Dai, D. Meng, X. H. Zhang, D. Qu, G. Liu, V. S. Battaglia and Z. Y. Tang, *ACS Appl Mater Interfaces*, 2015, **7**, 12057-12066.
33. J.-P. Jegal and K.-B. Kim, *J Power Sources*, 2013, **243**, 859-864.
34. D. Yaakov, Y. Gofer, D. Aurbach and I. C. Halalay, *J Electrochem Soc*, 2010, **157**, A1383-A1391.
35. Y. H. Ren, C. W. Yang, B. R. Wu, C. Z. Zhang, S. Chen and F. Wu, *Advanced Materials Research*, 2011, **287-290**, 1283-1289.
36. B. Liu, B. Li and S. Guan, *Electrochemical and Solid-State Letters*, 2012, **15**, A77-A79.
37. S. Zhang, K. Xu, J. Allen and T. Jow, *J Power Sources*, 2002, **110**, 216-221.
38. Y. Jiang, W. Xu, D. Chen, Z. Jiao, H. Zhang, Q. Ma, X. Cai, B. Zhao and Y. Chu, *Electrochim Acta*, 2012, **85**, 377-383.
39. C. Chang, J. Xiang, X. Shi, X. Han, L. Yuan and J. Sun, *Electrochim Acta*, 2008, **54**, 623-627.
40. Y.Q. Qiao, X.L. Wang, J.Y. Xiang, D. Zhang, W.L. Liu and J.P Tu, *Electrochim Acta*, 2011, **56**, 2269-2275.
41. L. Wang, X. Zhou and Y. Guo, *J Power Sources*, 2010, **195**, 2844-2850.
42. K. Wu, *Ionics*, 2011, **18**, 55-58.
43. F. Wu, F. Wang, C. Wu and Y. Bai, *J Alloy Compd*, 2012, **513**, 236-241.
44. M. C. Smart, B. V. Ratnakumar, K. B. Chin and L. D. Whitcanack, *J Electrochem Soc*, 2010, **157**, A1361-A1374.

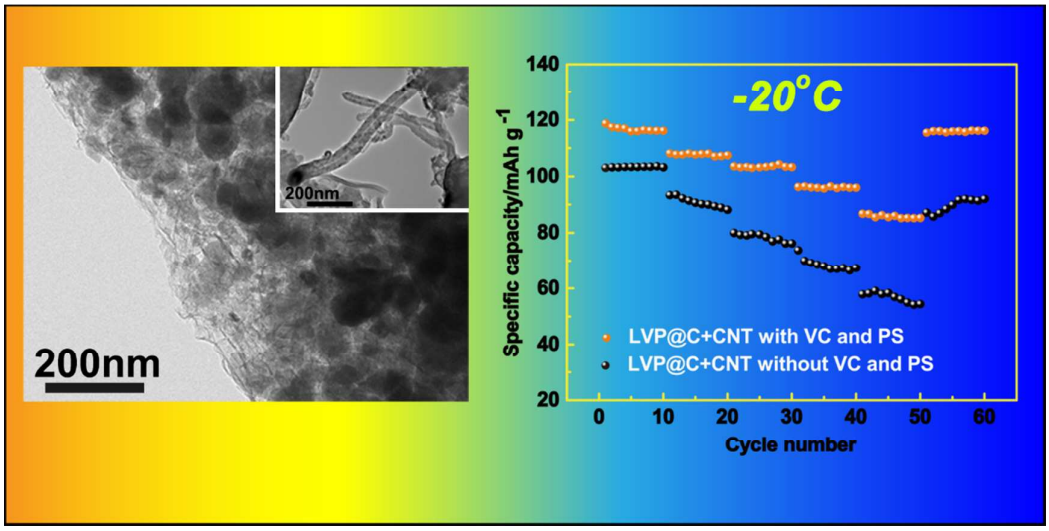

CNTs coating combined with the optimized electrolyte are introduced to improve the low temperature performances of $Li_3V_2(PO_4)_3$.